

NONSTATIONARY SPATIAL PROCESS MODELING VIA TREED COVARIATE SEGMENTATION, WITH APPLICATION TO SOIL ORGANIC CARBON STOCK ASSESSMENT

BY MARK D. RISSER^{*}, CATHERINE A. CALDER[†], VERONICA J. BERROCAL[‡], AND CANDACE BERRETT[§]

Lawrence Berkeley National Laboratory^{}, The Ohio State University[†], University of Michigan[‡], and Brigham Young University[§]*

Soil organic carbon (SOC), a generic term for the carbon found in soil's organic matter, is one of earth's most dynamic carbon reservoirs and is relevant for climate science, forestry, agriculture, and soil science. Accurate estimates of SOC are important for verifying carbon sequestration in soil, national carbon inventories, and climate change mitigation programs like carbon trading. Unfortunately, collection of SOC data is limited by time and cost constraints; therefore, statistical methods are necessary for estimating the spatial distribution of SOC. In this paper, we develop a spatial statistical method that involves modeling the second-order nonstationarity in SOC via relevant covariate processes. As these processes are not fully observed, we incorporate Bayesian CART for treed covariate segmentation in a manner that allows the first- and second-order properties of SOC to be similar in regions where the distribution of a covariate is homogeneous. Using Bayesian model averaging to account for uncertainty in the segmentation process and to accommodate multiple covariate processes, we outline an algorithm for generating predictions of SOC at unobserved locations based on our covariate-driven nonstationary model. Compared to related approaches, our method yields moderate improvements for out-of-sample cross validation and much faster computation relative to traditional spatial models.

1. Introduction. Oceans, terrestrial systems, and the atmosphere form the three primary carbon reservoirs on the earth (Batjes, 1996). The amount of carbon in terrestrial ecosystems is nearly three times that of the atmosphere, and while its size is dwarfed by the ocean's carbon storage, terrestrial carbon is much more dynamic (Batjes, 1996). Soil organic carbon (SOC), a generic term for the carbon found in soil's organic matter, constitutes approximately two-thirds of the carbon in terrestrial ecosystems and is an important component in the earth's carbon cycle (Post et al., 1982). The carbon in soil is in continuous interaction with the atmosphere via processes such as plant growth and decomposition (Bliss et al., 2014), and SOC helps

Keywords and phrases: Gaussian process, model averaging, nonstationary spatial modeling, soil carbon, spatial regression, treed segmentation

mitigate the negative consequences of global changes in climate by absorbing carbon released into the atmosphere by fossil fuel combustion (Jobbágy and Jackson, 2000; Post et al., 1982). In addition to its relevance to the earth’s climate, SOC is important in forestry and agriculture, as organic matter contributes to soil fertility by helping retain moisture and supply plant nutrients (Bliss et al., 2014; Post and Kwon, 2000). Furthermore, SOC is one of the soil properties used by hydrologists to better understand how precipitation is processed by different land surfaces and contributes to surface and ground water quality (Bliss et al., 2014).

Because of its broad relevance in climate and agriculture, it is increasingly important to obtain accurate estimates of SOC across space. For example, estimates of SOC are needed to quantify the carbon holding capacity of soil; furthermore, establishing equitable carbon trading programs (in which a country with higher carbon dioxide emissions purchases the right to emit more CO₂ from a country with lower emissions) requires precise measurements of SOC (Mishra et al., 2009). Estimates of SOC over space with corresponding uncertainties are necessary for national carbon inventories (Soloman, 2007). However, the collection of SOC data is highly limited by time and cost constraints (Sleutel et al., 2003; Goidts and van Wesemael, 2007), motivating the need for methods to predict SOC at unobserved locations. Prediction is typically performed using regression models, which relate the first-order properties of SOC to explanatory variables such as drainage class and land use (Meersmans et al., 2008), as well as terrain attributes (Minasny et al., 2006). In order to take advantage of spatial dependence in SOC, Simbahan et al. (2006) use kriging-based methods for predicting SOC.

Focusing on spatial prediction of SOC, we propose a statistical model that combines the strengths of each of the aforementioned methods: incorporating the spatial correlation innate to SOC, as well as leveraging the relationship between SOC and explanatory variables. While geostatistical methods have previously been used to accomplish these goals, existing approaches have relied on assumptions of second-order stationarity. Because SOC shows second-order nonstationary behavior on regional scales (see Section 2), our approach will instead allow the spatial dependence structure to vary over space. Furthermore, since it is well-documented that SOC is impacted by covariate information such as land use (Jobbágy and Jackson, 2000) and soil properties (Mishra et al., 2009), we set out to build a parametric model that uses these covariates to describe the first- and second-order nonstationarity in the spatial process. In terms of modeling the second-order nonstationarity, we build on the diverse literature of covariate-driven nonstationary spatial modeling (Calder, 2008, Schmidt, Guttorp and O’Hagan, 2011, Reich et al., 2011, Vianna Neto, Schmidt and Guttorp, 2014, Ingebrigtsen, Lindgren and Steinsland, 2014, Risser and Calder, 2015). Complicating matters in our setting, the covariates are not observed everywhere a prediction is desired, a requirement for the application of these existing covariate-driven nonstationary spa-

tial models. Our proposed methodology addresses this requirement through a novel spatial partitioning approach to nonstationary spatial modeling. Spatially-referenced covariates are used to define an informative prior on the distribution of random partitions of the study region. Using the covariates in this manner allow us to readily make predictions of SOC at locations where the covariates are not observed.

The paper proceeds as follows. In Section 2, we introduce the SOC data set and explanatory variables; Section 3 outlines the Bayesian statistical approach we developed for modeling SOC. An algorithm for model fitting and generating predictions of SOC at unobserved locations is described in Section 4. In Section 5 we present the results of our fitted model and predictions, and discuss the computational benefits which naturally arise from the structure of the model. Section 6 presents an evaluation of our method by comparing it to related procedures, and Section 7 concludes the paper.

2. Soil organic carbon data. The methodology described in this paper was developed to model a data set from the National Resources Conservation Service (NRCS) (available online; see [Wills et al., 2013](#)) that consists of measurements of SOC obtained as part of the Rapid Carbon Assessment (RaCA) project. The RaCA project, initiated by the Soil Science Division (SSD) of NRCS, had the goal of capturing information on the carbon content of soils across the conterminous United States at a single point in time. RaCA specifically emphasizes SOC stocks, i.e., the amount of SOC in a volume (area and depth of soil). Additional variables such as land use-land cover (LULC) classes, soil series, and soil moisture are available through the `soilDB` package in R ([Beaudette and Skovlin, 2015](#)), and a summary report of the sampling methods and data description is provided in [Wills et al. \(2013\)](#). While measurements of SOC stocks are available for each site to depths of five, ten, twenty, thirty, fifty, and one hundred centimeters (in MG C ha^{-1}), we will use the one hundred centimeter depth measurement since our focus is on estimating total SOC, not a soil depth profile (e.g., [Minasny et al., 2006](#); [Mishra et al., 2009](#)).

In order to be able to compare our proposed methodology with “traditional” spatial Gaussian process models that make assumptions of second-order stationarity, instead of setting out to model the entire data set (which contains approximately 6400 observations) we focus on a subset of the SOC data set corresponding to the Great Lakes region of the midwestern United States, shown in Figure 1, which contains 790 observations. For a data set of size n , standard Gaussian process model calculations involve repeatedly taking the inverse and determinant of an $n \times n$ matrix, which requires $\mathcal{O}(n^3)$ time and $\mathcal{O}(n^2)$ memory complexity: this is (relatively) feasible for $n = 790$ but not $n \approx 6400$. This subset was chosen as the rectangular region that contains Ohio, Indiana, Illinois, Wisconsin, and Michigan.

2.1. Exploratory analysis. As discussed in Section 1, accurate estimation of the spatial distribution of SOC is hindered by costly and time-consuming data collection,

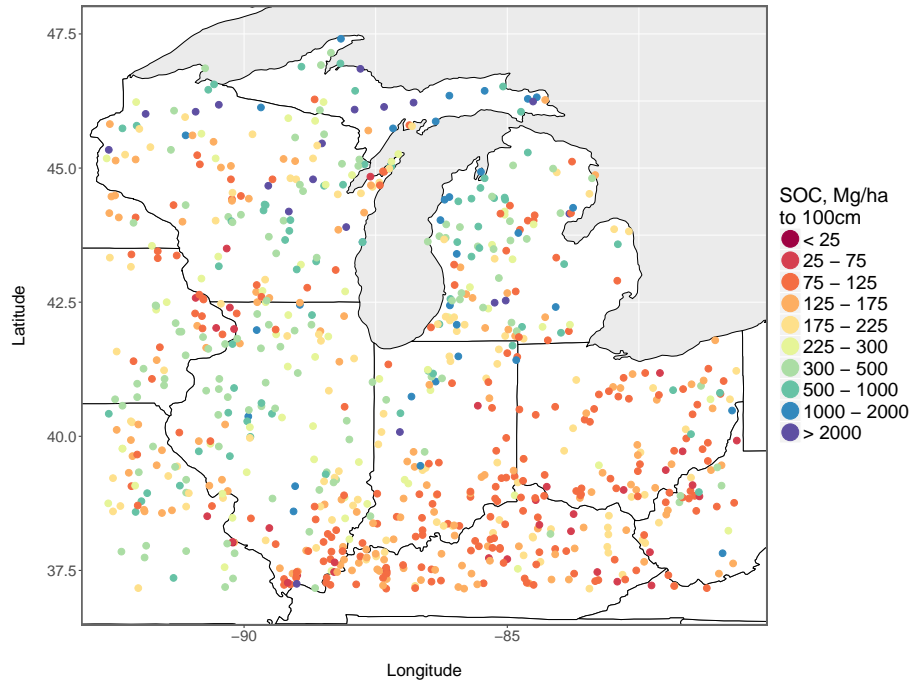


FIG 1. *Great Lakes subset of the soil organic carbon stocks data set.*

and we are thus motivated to consider spatial statistical methods to predict SOC at unobserved locations. Focusing on the Great Lakes subregion, we begin with a simple variogram analysis of the SOC data, first calculating the empirical semivariogram and corresponding fitted exponential semivariogram for the entire region (here and throughout the remainder of the paper, the SOC data is transformed to the log scale; for the variogram analyses, we use the OLS residuals from a regression of log SOC on latitude, longitude, and the longitude/latitude interaction); as can be seen from plot (b) in Figure 2, the exponential model fits the empirical semivariogram quite well. Now, consider the corresponding analysis when we arbitrarily divide the spatial domain into four parts and fit separate variograms to each subregion; see plots (c) and (d) of Figure 2. The variograms (empirical and fitted) indicate that the subregions display quite different spatial dependence patterns.

These differences motivate a nonstationary spatial model for the SOC data, which allows the spatial dependence properties to vary over the spatial domain. However, the arbitrary partitioning of the Great Lakes region (as in Figure 2) is not scientifically meaningful, and fitting separate variograms for different subregions does not comprise a desirable spatial model as no information is shared across the subregions. Therefore,

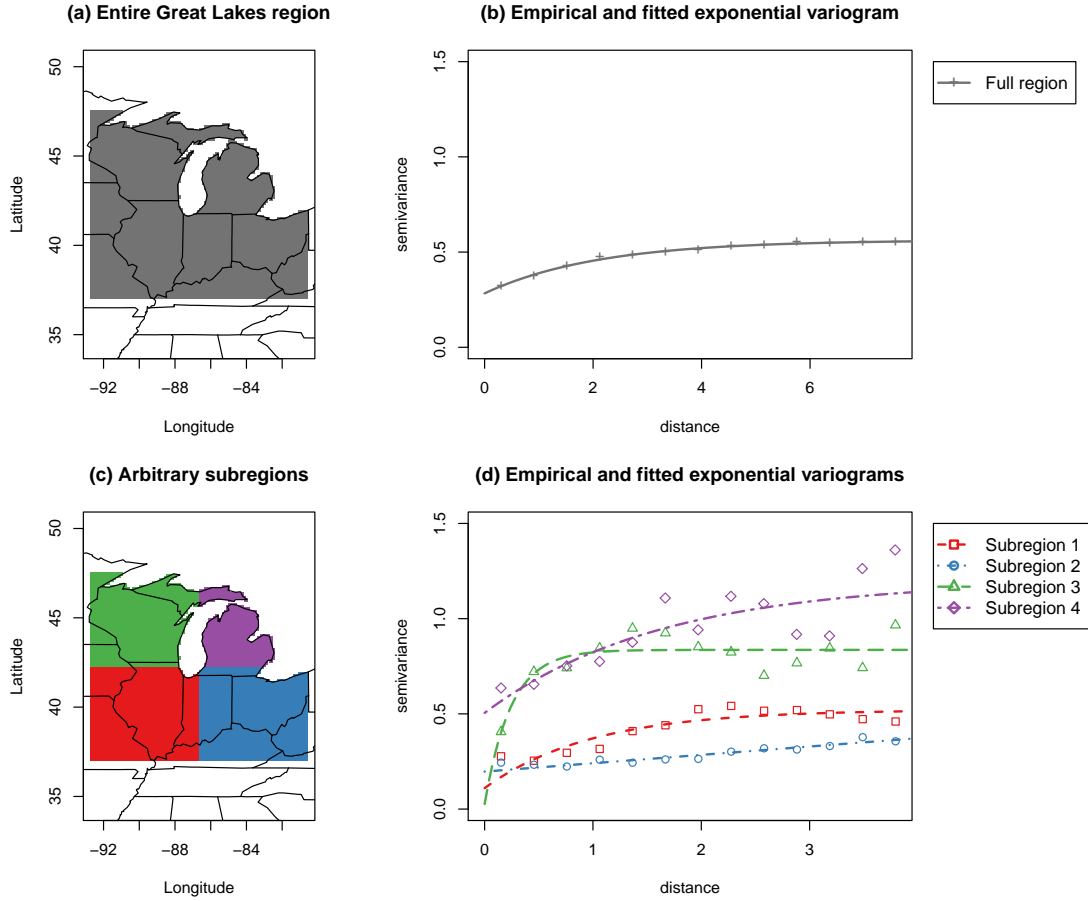


FIG 2. Empirical (points) and fitted (lines) exponential variograms for the entire Great Lakes region (top) and for four arbitrary subregions (bottom).

we are motivated to consider an alternative approach.

2.2. Covariate information. As discussed in Section 1, there are well-documented relationships between SOC and a number of covariate variables, for example, land use-land cover (LULC) class and drainage class. Both of these categorical variables are available in the `soilDB` package in R (Beaudette and Skovlin, 2015). As outlined in Wills et al. (2013), the LULC classes were developed specifically for the RaCA project to correspond to the classes and definitions of the Natural Resources Inventory. RaCA designated five specific LULC classes (four of which are represented in the Great Lakes region subset), namely cropland, farmland, pastureland, rangeland, and wetland, with

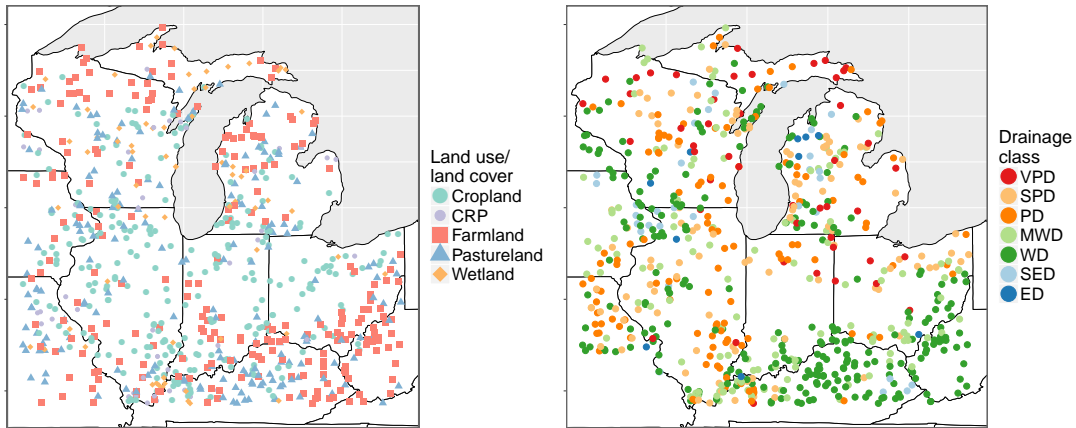


FIG 3. The Great Lakes region subset of the Rapid Carbon Assessment (RaCA) land use-land cover classes (left) and drainage classes. For land use, CRP refers to a Conservation Reserve Program cropland site. For drainage class, the labels are as follows: VPD = very poorly drained, SPD = somewhat poorly drained, PD = poorly drained, MWD = moderately well drained, WD = well drained, SED = somewhat excessively drained, ED = excessively drained.

one additional category for any cropland site that was also known to correspond to a Conservation Reserve Program (CRP). The drainage class variable refers to “the frequency and duration of wet periods under conditions similar to those under which the soil developed. Alteration of the water regime by man, either through drainage or irrigation, is not a consideration unless the alterations have significantly changed the morphology of the soil” (NRCS Soil Survey Manual, chapter 3). Plots of the subsetted LULC and drainage class variables are shown in Figure 3.

Given the known scientific relationships between SOC and these variables as well as the rich literature of covariate-driven nonstationary modeling, we wish to leverage these covariates within the spatial model. In other words, our hypothesis is that both the first- and second-order properties of SOC might be the same in areas where the covariates are homogeneous. However, for LULC and drainage class, the relevant covariate information is not available for every prediction location (or even observed location) of interest. As such, the nonstationary models of Reich et al. (2011), Vianna Neto, Schmidt and Guttorp (2014), Ingebrigtsen, Lindgren and Steinsland (2014), and Risser and Calder (2015) cannot be used, unless the covariate itself can somehow be smoothed over space (as in Vianna Neto, Schmidt and Guttorp, 2014). But, since we wish to allow the covariates to drive the first- and/or second-order properties, this may not be desirable or even possible for a categorical covariate.

To overcome this limitation, instead of directly including the covariate values into the model (as in Reich et al., 2011, Ingebrigtsen, Lindgren and Steinsland, 2014, and

(Risser and Calder, 2015), we propose using a segmentation or clustering approach that uses the available covariate information to divide the spatial domain into segments based on the distribution of the covariate within each segment. Once defined, the segments partition the domain such that every location is contained in exactly one of these segments, and the process within each segment is assumed to be homogeneous: using segment-specific regression coefficients (first-order homogeneity) and/or requiring that the process be (locally) stationary within the segment (second-order homogeneity). In other words, it is the segment membership that will be used in our statistical model, not the value of the covariate. We now outline an approach that yields such a model.

3. A nonstationary spatial Gaussian process model. Let $Z(\cdot)$ represent log SOC, where we model $Z(\cdot)$ as a spatial stochastic process defined for all $\mathbf{s} \in \mathcal{D}$, where \mathcal{D} denotes the Great Lakes region of the United States. Then, suppose we observe the value of $Z(\cdot)$ at a fixed, finite set of locations $\{\mathbf{s}_1, \mathbf{s}_2, \dots, \mathbf{s}_n\} \in \mathcal{D}$ and wish to use these observations to learn about the underlying process. For all $\mathbf{s} \in \mathcal{D}$, let

$$(3.1) \quad Z(\mathbf{s}) = \mu(\mathbf{s}) + Y(\mathbf{s}) + \epsilon(\mathbf{s}),$$

where $E[Z(\mathbf{s})] = \mu(\mathbf{s})$ is a deterministic mean function, $Y(\cdot)$ is a mean-zero latent spatial (Gaussian) process, and $\epsilon(\cdot)$ is an error process that is assumed to be independent of $Y(\cdot)$. See Section 5.2 for further details on $\mu(\cdot)$.

Because the latent Gaussian process $Y(\cdot)$ is mean-zero, we simply need to specify a model for its covariance function C , which describes the covariance between the process at two locations: $C(\mathbf{s}, \mathbf{s}') \equiv \text{Cov}(Y(\mathbf{s}), Y(\mathbf{s}'))$ for $\mathbf{s}, \mathbf{s}' \in \mathcal{D}$. Recall that we want C to be nonstationary, such that $C(\mathbf{s}, \mathbf{s}') \neq C(\|\mathbf{s} - \mathbf{s}'\|)$; however, C must also be a valid covariance function (i.e., C must be even and non-negative definite; Bochner, 1959 and Adler, 1981) and also estimable from only a single realization of $Z(\cdot)$ (we have no repeated measurements of SOC). Of the wide variety of nonstationary covariance function models (e.g., Sampson and Guttorp, 1992; Higdon, 1998; Paciorek and Schervish, 2006; Lindgren, Rue and Lindstrom, 2011), we propose a model in the style of Fuentes (2001), which specifies a nonstationary model for $Y(\cdot)$ via a mixture of stationary processes

$$(3.2) \quad Y(\mathbf{s}) = \sum_{k=1}^K w_k(\mathbf{s}) \tilde{Y}_k(\mathbf{s}),$$

where the $\tilde{Y}_k(\cdot)$ are orthogonal (i.e., $\text{Cov}(\tilde{Y}_i(\mathbf{s}), \tilde{Y}_j(\mathbf{s}')) = 0$, for $i \neq j$) and stationary, and $w_k(\cdot)$ is a positive kernel weight function such that (following Reich et al., 2011) $w_k(\mathbf{s}) \geq 0$ and $\sum_{k=1}^K [w_k(\mathbf{s})]^2 = 1$ for all $\mathbf{s} \in \mathcal{D}$. For the covariance function \tilde{C}_k of each

$\tilde{Y}_k(\cdot)$, we use an anisotropic version of the parametric Matérn model

$$(3.3) \quad \tilde{C}_k(\mathbf{s} - \mathbf{s}'; \boldsymbol{\theta}_k) = \sigma_k^2 \frac{1}{\Gamma(\nu_k) 2^{\nu_k - 1}} \left[\sqrt{Q_k(\mathbf{s} - \mathbf{s}')} \right]^{\nu_k} \mathcal{K}_{\nu_k} \left(\sqrt{Q_k(\mathbf{s} - \mathbf{s}')} \right).$$

In (3.3), $\mathcal{K}_{\nu_k}(\cdot)$ denotes the modified Bessel function of the third kind of order ν_k , $Q_k(\mathbf{s} - \mathbf{s}') = \|\boldsymbol{\Sigma}_k^{-1/2}(\mathbf{s} - \mathbf{s}')\|^2$ is a squared Mahalanobis distance with anisotropy matrix $\boldsymbol{\Sigma}_k$ parameterized according to its spectral decomposition, i.e. (for $d = 2$),

$$(3.4) \quad \boldsymbol{\Sigma}_k = \begin{bmatrix} \cos(\eta_k) & -\sin(\eta_k) \\ \sin(\eta_k) & \cos(\eta_k) \end{bmatrix} \begin{bmatrix} \phi_{1k} & 0 \\ 0 & \phi_{2k} \end{bmatrix} \begin{bmatrix} \cos(\eta_k) & \sin(\eta_k) \\ -\sin(\eta_k) & \cos(\eta_k) \end{bmatrix},$$

and $\boldsymbol{\theta}_k = (\sigma_k^2, \nu_k, \phi_{1k}, \phi_{2k}, \eta_k)$ is a vector of parameters that control the spatial dependence properties of $\tilde{Y}_k(\cdot)$ (e.g., variance, smoothness, anisotropy). In the anisotropy matrices (3.4), ϕ_{1k} and ϕ_{2k} represent directional ‘‘ranges’’ (i.e., inverse decay parameters) and η_k represents an angle of rotation; these parameters allow for locally elliptical correlation patterns. The resulting covariance function for (3.2) is $C(\mathbf{s}, \mathbf{s}') = \sum_{k=1}^K w_k(\mathbf{s}) w_k(\mathbf{s}') \tilde{C}_k(\mathbf{s} - \mathbf{s}'; \boldsymbol{\theta}_k)$, which is a nonstationary covariance function.

To complete the specification of our model (3.1), we suppose that the error process $\epsilon(\mathbf{s})$ is spatially independent and Gaussian. Similar to (3.2), we model $\epsilon(\mathbf{s}) = \sum_{k=1}^K w_k(\mathbf{s}) \tilde{\epsilon}_k(\mathbf{s})$, where each $\tilde{\epsilon}_k(\mathbf{s}) \stackrel{\text{iid}}{\sim} N(0, \tau_k^2)$. Thus, we expand the $\boldsymbol{\theta}_k$ vector to include the variance τ_k^2 .

Often, the weight functions $w_k(\cdot)$ are chosen to be indicator functions for one piece of a partition of \mathcal{D} , or $w_k(\mathbf{s}) = \mathbb{1}(\mathbf{s} \in D_k)$ (e.g., Gramacy and Lee, 2008), where we suppose there exists a process \mathcal{T} that partitions \mathcal{D} into distinct, non-overlapping subregions $\{D_k : k = 1, \dots, K\}$, such that each $\mathbf{s} \in \mathcal{D}$ lies in exactly one of the D_k . In this case the process $Y(\cdot)$, and therefore also $Z(\cdot)$, is now locally stationary within each D_k and also independent across the D_k , conditional on \mathcal{T} . For the random observed vector $\mathbf{Z} \equiv (Z(\mathbf{s}_1), \dots, Z(\mathbf{s}_n))^\top$, the indicator weight function implies a conditional likelihood for \mathbf{Z} ,

$$(3.5) \quad p(\mathbf{Z} | \boldsymbol{\mu}, \boldsymbol{\theta}, \mathcal{T}) \propto \prod_{k=1}^K |\mathbf{V}_k + \boldsymbol{\Omega}_k|^{-1/2} \times \exp \left\{ -\frac{1}{2} (\mathbf{Z}_k - \boldsymbol{\mu}_k)^\top (\mathbf{V}_k + \boldsymbol{\Omega}_k)^{-1} (\mathbf{Z}_k - \boldsymbol{\mu}_k) \right\},$$

which is the product of segment-specific multivariate Gaussian likelihoods. In (3.5), the ‘‘ k ’’ subscript partitions each term into its segment-specific components, e.g., $\mathbf{Z}_k = \{Z(\mathbf{s}_i) : \mathbf{s}_i \in D_k\}$; $\mathbf{V}_k = \tau_k^2 \mathbf{I}$ captures a segment-specific measurement error variance; the elements of $\boldsymbol{\Omega}_k$ come from \tilde{C}_k . Note that the likelihood for \mathbf{Z} in (3.5) is *conditional* on the process \mathcal{T} . As a result, the segmentation process controls both the first- and second-order properties of $Z(\cdot)$, as desired: the mean vector $\boldsymbol{\mu}$ is divided into segment-specific components and, of course, the segmentation determines independent regions of local stationarity.

Therefore, we have motivation to specify a tree or segmentation model for \mathcal{T} which, in a Bayesian setting, involves specifying a prior distribution for the segmentation process \mathcal{T} . Because the segmentation process controls the properties of $Z(\cdot)$, we seek a model that incorporates meaningful scientific information via covariates. Returning to our hypothesis that the second-order properties of SOC might be the same in areas where the LULC and drainage class covariates are homogeneous, we can use a segmentation model on the covariates to define a prior for \mathcal{T} . One approach for doing so is Bayesian classification and regression trees (Bayesian CART, [Chipman, George and McCulloch, 1998](#)). If the covariates drive the second-order properties of the spatial process, then the distribution of the covariates over geographic space could be used to determine a partitioning of the spatial domain, since this partitioning controls the local properties of the spatial process.

In other words, we propose using Bayesian CART with the *covariates* LULC and drainage class as the response variable (hence the “treed covariate segmentation” terminology) to construct our prior for \mathcal{T} . Defining \mathbf{Z}_T to be a vector of covariates to be used as the response for the treed model ($\mathbf{Z}_T = \text{LULC or drainage class}$), [Chipman, George and McCulloch \(1998\)](#) introduce a Markov chain Monte Carlo algorithm to simulate a sequence of trees $\mathcal{T}_0, \mathcal{T}_1, \mathcal{T}_2, \dots$ that converges in distribution to the posterior $p(\mathcal{T}|\mathbf{Z}_T = \mathbf{z}_T)$. The details of this algorithm have been well-developed in the literature (see, e.g., [Chipman, George and McCulloch, 1998](#)); for more details, see [Appendix A](#). Our approach continues by constructing the segmentation prior $p(\mathcal{T})$ from the Bayesian CART posterior $p(\mathcal{T}|\mathbf{Z}_T = \mathbf{z}_T)$.

4. Bayesian posterior prediction and model fitting. Recall from [Section 1](#) that our primary goal for using this model is prediction. Define a collection of locations $\{\mathbf{s}_1^*, \dots, \mathbf{s}_m^*\} \subset \mathcal{D}$ for which we would like to obtain predictions of the corresponding (log) SOC values $\mathbf{Z}^* = (Z(\mathbf{s}_1^*), \dots, Z(\mathbf{s}_m^*))$. Using a Bayesian framework, the posterior predictive distribution for \mathbf{Z}^* conditional on observed $\mathbf{Z} = \mathbf{z}$ is then

$$(4.1) \quad \begin{aligned} p(\mathbf{Z}^*|\mathbf{Z} = \mathbf{z}) &= \int p(\mathbf{Z}^*, \boldsymbol{\mu}, \boldsymbol{\theta}, \mathcal{T}|\mathbf{Z} = \mathbf{z}) d\mathcal{T} d\boldsymbol{\theta} d\boldsymbol{\mu} \\ &= \int p(\mathbf{Z}^*|\boldsymbol{\mu}, \boldsymbol{\theta}, \mathcal{T}, \mathbf{Z} = \mathbf{z}) p(\boldsymbol{\mu}, \boldsymbol{\theta}, \mathcal{T}|\mathbf{Z} = \mathbf{z}) d\mathcal{T} d\boldsymbol{\theta} d\boldsymbol{\mu}. \end{aligned}$$

Because we are using a Gaussian process model, $p(\mathbf{Z}^*|\boldsymbol{\mu}, \boldsymbol{\theta}, \mathcal{T}, \mathbf{Z} = \mathbf{z})$ is multivariate Gaussian: with

$$\begin{bmatrix} \mathbf{Z} \\ \mathbf{Z}^* \end{bmatrix} \Big| \boldsymbol{\mu}, \boldsymbol{\theta}, \mathcal{T} \sim N_{n+m} \left(\begin{bmatrix} \boldsymbol{\mu} \\ \boldsymbol{\mu}^* \end{bmatrix}, \begin{bmatrix} \mathbf{V} + \boldsymbol{\Omega} & \boldsymbol{\Omega}_{\mathbf{Z}\mathbf{Z}^*} \\ \boldsymbol{\Omega}_{\mathbf{Z}^*\mathbf{Z}} & \mathbf{V}^* + \boldsymbol{\Omega}^* \end{bmatrix} \right),$$

where $\boldsymbol{\Omega}_{\mathbf{Z}^*\mathbf{Z}} \equiv \text{Cov}(\mathbf{Z}^*, \mathbf{Z})$, it follows that

$$(4.2) \quad p(\mathbf{Z}^*|\boldsymbol{\mu}, \boldsymbol{\theta}, \mathcal{T}, \mathbf{Z} = \mathbf{z}) = N_m(\boldsymbol{\mu}_{\mathbf{Z}^*|\mathbf{z}}, \boldsymbol{\Sigma}_{\mathbf{Z}^*|\mathbf{z}}),$$

where $\boldsymbol{\mu}_{\mathbf{Z}^*|\mathbf{z}} = \boldsymbol{\mu}^* + \boldsymbol{\Omega}_{\mathbf{Z}^*\mathbf{z}}(\mathbf{V} + \boldsymbol{\Omega})^{-1}(\mathbf{z} - \boldsymbol{\mu})$ and $\boldsymbol{\Sigma}_{\mathbf{Z}^*|\mathbf{z}} = (\mathbf{V}^* + \boldsymbol{\Omega}^*) - \boldsymbol{\Omega}_{\mathbf{Z}^*\mathbf{z}}(\mathbf{V} + \boldsymbol{\Omega})^{-1}\boldsymbol{\Omega}_{\mathbf{z}\mathbf{Z}^*}$. The other component in (4.1) is the posterior distribution $p(\boldsymbol{\mu}, \boldsymbol{\theta}, \mathcal{T}|\mathbf{Z}) \propto p(\mathbf{Z}|\boldsymbol{\mu}, \boldsymbol{\theta}, \mathcal{T})p(\boldsymbol{\mu}, \boldsymbol{\theta}|\mathcal{T})p(\mathcal{T})$, where $p(\mathbf{Z}|\boldsymbol{\mu}, \boldsymbol{\theta}, \mathcal{T})$ is the likelihood from (3.5), the priors for $\boldsymbol{\mu}$ and $\boldsymbol{\theta}$ are conditional on the segmentation \mathcal{T} , and $p(\mathcal{T})$ is constructed from the Bayesian CART posterior $p(\mathcal{T}|\mathbf{Z}_T = \mathbf{z}_T)$. See Section 5.2 for more details on $p(\boldsymbol{\mu}, \boldsymbol{\theta}|\mathcal{T})$.

While sampling from $p(\boldsymbol{\mu}, \boldsymbol{\theta}, \mathcal{T}|\mathbf{Z} = \mathbf{z})$ is quite complicated, it is relatively straightforward to sample from $p(\boldsymbol{\mu}, \boldsymbol{\theta}|\mathcal{T}, \mathbf{Z} = \mathbf{z})$. With the posterior predictive distribution (4.1) as our goal, note that we can rewrite the posterior as $p(\boldsymbol{\mu}, \boldsymbol{\theta}, \mathcal{T}|\mathbf{Z} = \mathbf{z}) = p(\boldsymbol{\mu}, \boldsymbol{\theta}|\mathcal{T}, \mathbf{Z} = \mathbf{z}) \times p(\mathcal{T}|\mathbf{Z} = \mathbf{z})$, so that (4.1) becomes

$$p(\mathbf{Z}^*|\mathbf{Z} = \mathbf{z}) = \int p(\mathbf{Z}^*|\boldsymbol{\mu}, \boldsymbol{\theta}, \mathcal{T}, \mathbf{Z} = \mathbf{z})p(\boldsymbol{\mu}, \boldsymbol{\theta}|\mathcal{T}, \mathbf{Z} = \mathbf{z})p(\mathcal{T}|\mathbf{Z} = \mathbf{z})d\mathcal{T}d\boldsymbol{\theta}d\boldsymbol{\mu}.$$

This suggests the following algorithm to sample from $p(\mathbf{Z}^*|\mathbf{Z} = \mathbf{z})$:

Posterior Prediction Algorithm (PPA)

1. Draw \mathcal{T}^* from $p(\mathcal{T}|\mathbf{Z} = \mathbf{z})$.
2. Draw $(\boldsymbol{\mu}^*, \boldsymbol{\theta}^*)$ from $p(\boldsymbol{\mu}, \boldsymbol{\theta}|\mathcal{T} = \mathcal{T}^*, \mathbf{Z} = \mathbf{z})$, which is the posterior distribution for the mean and covariance parameters conditional on \mathcal{T}^* .
3. Draw \mathbf{Z}^* from $p(\mathbf{Z}^*|\boldsymbol{\mu} = \boldsymbol{\mu}^*, \boldsymbol{\theta} = \boldsymbol{\theta}^*, \mathcal{T} = \mathcal{T}^*, \mathbf{Z} = \mathbf{z})$, defined in (4.2).

In order to implement the above algorithm, we select a total of J segmentations $\{\mathcal{T}_j : j = 1, \dots, J\}$ which have both high posterior probability conditional on the covariates (i.e., high $p(\mathcal{T}|\mathbf{Z}_T = \mathbf{z}_T)$) and are representative of the full collection of posterior samples. These representative segmentations can be used to define the support for a discrete uniform prior

$$(4.3) \quad p(\mathcal{T}) = \frac{1}{J} \sum_{j=1}^J \mathbb{1}(\mathcal{T} = \mathcal{T}_j),$$

so that step 2 of the above algorithm is feasible. As such, step 1 of the above algorithm actually involves drawing $\mathcal{T}^* \in \{\mathcal{T}_1, \dots, \mathcal{T}_J\}$ according to $p(\mathcal{T}|\mathbf{Z} = \mathbf{z})$.

Sampling from the posterior predictive distribution using the PPA complicates matters in that we need to calculate the marginal probabilities $p(\mathcal{T}_j|\mathbf{Z} = \mathbf{z})$ for $j = 1, \dots, J$, but greatly simplifies model fitting overall by allowing us to generate samples from each of the conditional posteriors $p(\boldsymbol{\mu}, \boldsymbol{\theta}|\mathcal{T} = \mathcal{T}^*, \mathbf{Z} = \mathbf{z})$ ahead of time, and in parallel. Using Bayes Theorem, the posterior probability of each segmentation conditional on the data is

$$(4.4) \quad p(\mathcal{T}_j|\mathbf{Z} = \mathbf{z}) = \frac{p(\mathbf{Z}|\mathcal{T}_j)p(\mathcal{T}_j)}{\sum_{i=1}^J p(\mathbf{Z}|\mathcal{T}_i)p(\mathcal{T}_i)} = \frac{p(\mathbf{Z}|\mathcal{T}_j)}{\sum_{i=1}^J p(\mathbf{Z}|\mathcal{T}_i)},$$

where the last equality comes from the uniform specification in (4.3). So, the important quantity is actually the marginal likelihood

$$(4.5) \quad p(\mathbf{Z}|\mathcal{T}_j) = \int p(\mathbf{Z}|\boldsymbol{\mu}, \boldsymbol{\theta}, \mathcal{T}_j)p(\boldsymbol{\mu}, \boldsymbol{\theta}|\mathcal{T}_j)d\boldsymbol{\theta}d\boldsymbol{\mu}.$$

Estimation of the marginal likelihood $p(\mathbf{Z}|\mathcal{T}_j)$ is a well-known problem in Bayesian analysis; for more details on our approach, see Appendix B.

Combining all of the above, the model fitting uses the following procedure:

Model Fitting Algorithm (MFA)

1. Use the MCMC algorithm described in Appendix A to obtain segmentations based on one or more covariate values and choose a collection of segmentations $\{\mathcal{T}_1, \dots, \mathcal{T}_J\}$ to use for the model averaging (see Section 5 for more details on this step).
2. For each of the J selected segmentations, use standard MCMC methods to obtain posterior samples of the mean and covariance parameters from $p(\boldsymbol{\mu}, \boldsymbol{\theta}|\mathcal{T}, \mathbf{Z} = \mathbf{z})$.
3. Estimate the marginal likelihoods and calculate the $p(\mathcal{T}_j|\mathbf{Z} = \mathbf{z})$.
4. Sample from the posterior predictive distribution using PPA.

5. Results.

5.1. *Segmentation selection.* Candidate segmentations for the model averaging are based on the land use and drainage class variables, and are obtained from the Metropolis-Hastings algorithm outlined in Appendix A. In order to extract a more diverse set of candidates, we obtained segmentations using rotated coordinates, in which the coordinate axes were rotated by angles of 0, $\pi/6$, and $\pi/3$. Finally, two segmentation resolutions were considered: coarse, with three or four segments, and fine, with six or seven segments.

When running the Bayesian CART MCMC, we ran into a problem similar to what Chipman, George and McCulloch (1998) found: the Markov chain navigates quickly to a region of large posterior probability and subsequently moves locally within the region for a long time. To avoid running extremely long Markov chains, Chipman, George and McCulloch (1998) recommend restarting the algorithm multiple times and collecting the posterior samples from each restart into a larger collection of samples which represent the different local modes of the posterior. This strategy will yield a large number of candidate segmentations, probably much larger than is desired for the model averaging strategy in Section 4. In order to select a smaller, more reasonable subset of segmentations to use in the model averaging, we again follow the recommendation given in Chipman, George and McCulloch (1998), which is to pick out the segmentations with the largest likelihood. Multidimensional scaling (MDS) was used to embed the pool of candidate segmentations in \mathbb{R}^1 and “representative” segmentations were

selected from the empirical distribution of the embedded points. The distance metric used for the MDS was a Jaccard distance between sets binary indicators of whether pairs of points on a regular grid covering the study region fall in the same segment of a particular segmentation. This procedure ensured that the selected segmentations were representative of the full posterior and not too similar to each other.

For this application, a slight change was made to the algorithm for generating candidate segmentations. Because we need to fit a separate stationary (anisotropic) model within each segment, the size of the segment needs to be large enough (both in size and in number of observations) to efficiently estimate all of the parameters of the stationary spatial model. So, a simple change was made within the Metropolis-Hastings, in that a candidate segmentation was rejected if any of the segments were either (a) smaller than a $1^\circ \times 1^\circ$ longitude-latitude region or (b) contained fewer than twenty observations.

The Metropolis-Hastings algorithm was restarted many times for each covariate variable, using the tree prior hyperparameters $\alpha_T = 0.5$ and $\beta_T = 2$ (following Chipman, George and McCulloch, 1998). A total of $J = 20$ segmentations were selected for the model averaged predictions (and are plotted in Figure 4): ten coarse (1-10) and ten fine (11-20).

5.2. Mean function and hyperparameter specification. The general model introduced in Section 3 can accommodate any mean structure, including (in the case of a linear mean) fully observed covariates and categorical covariates based on the segmentation process (i.e., a separate mean or intercept for each segment). For log SOC, we considered a linear mean function including longitude, latitude, the interaction between longitude and latitude, and intercepts specific to segment membership as covariates; however, it was found that the model without latitude and longitude effects performed as well (if not better) than the model with a global mean latitude and longitude coefficients. Unfortunately, a mean function with only the segment membership as a covariate resulted in an undesirable discontinuous mean, so in our final implementation of the nonstationary model the mean function for each segmentation is simply a constant (i.e., $\boldsymbol{\mu} = \mu \mathbf{1}$).

For the prior distribution, we factorize $p(\boldsymbol{\mu}, \boldsymbol{\theta} | \mathcal{T}) = p(\boldsymbol{\mu} | \mathcal{T})p(\boldsymbol{\theta} | \mathcal{T})$. The prior on $\boldsymbol{\mu}$ is conjugate for the likelihood (3.5), i.e., $p(\boldsymbol{\mu} | \mathcal{T}) = N(0, \mathbf{c}_\mu^2)$; the prior for $\boldsymbol{\theta}$ is conditional on the segmentation since \mathcal{T} controls the dimension of $\boldsymbol{\theta}$:

$$(5.1) \quad p(\boldsymbol{\theta} | \mathcal{T}) = \prod_{k=1}^K p(\nu_k) p(\tau_k^2) p(\sigma_k^2) p(\phi_{1k}) p(\phi_{2k}) p(\eta_k)$$

(the conditioning on \mathcal{T} on the right hand side is suppressed). Each component of (5.1)

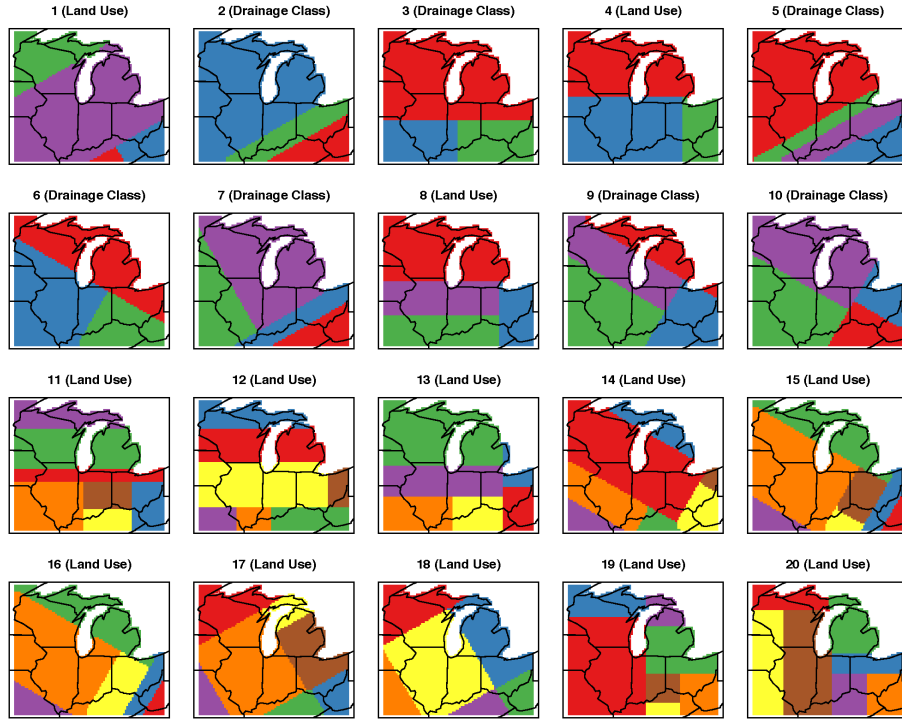


FIG 4. Final segmentations chosen for the model-averaged predictions. Segmentations 1-10 represent the coarse segmentations; 11-20 represent the fine.

is noninformative and proper: for $k = 1, \dots, K$,

$$\begin{aligned}
 p(\nu_k) &= \text{Uniform}(0, c_\nu), & p(\tau_k^2) &= \text{Uniform}(0, c_\tau), \\
 p(\sigma_k^2) &= \text{Uniform}(0, c_\sigma), & p(\phi_{1k}) &= \text{Uniform}(0, d_k), \\
 p(\phi_{2k}) &= \text{Uniform}(0, d_k), & p(\eta_k) &= \text{Uniform}[0, \pi/2]
 \end{aligned}$$

Uniform priors for the variance parameters τ^2 and σ^2 are used in place of more traditional (conjugate) inverse-Gamma priors to avoid prior bias in the case where an individual segment contains a small number of observations (following Gelman, 2006). The upper limits for the priors on the anisotropy matrix eigenvalues, ϕ_{1k} and ϕ_{2k} , which correspond to squared ranges of dependence, are determined by the size of the segment, i.e., $d_k = \max\{\|\mathbf{s} - \mathbf{s}'\| : \mathbf{s}, \mathbf{s}' \in D_k\}$, where D_k is the k th segment. The reasoning behind this choice is that the squared spatial range of the process within a segment is not expected to exceed the size of the segment. The limits on the prior for η_k are set to ensure identifiability (following, e.g., Katzfuss, 2013).

The fixed hyperparameters for $p(\mu|\mathcal{T})$ and $p(\theta|\mathcal{T})$ are summarized in Table 1. Based

TABLE 1

A summary of the hyperparameter values used to fit the nonstationary model.

Hyperparameter	Fixed value
c_β^2	100^2
c_τ	100
c_σ	100
d_k	$\max\{\ \mathbf{s} - \mathbf{s}'\ : \mathbf{s}, \mathbf{s}' \in D_k\}$

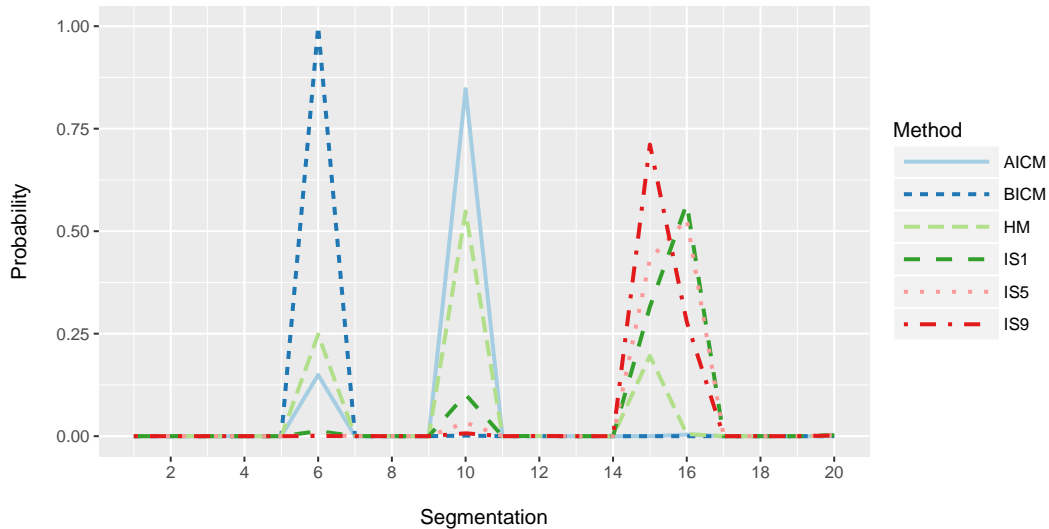


FIG 5. Posterior probabilities $p(\mathcal{T}|\mathbf{Z} = \mathbf{z})$ of each segmentation for each of several marginal likelihood estimation methods. AICM and BICM are Monte Carlo estimates of AIC and BIC, respectively (Raftery et al., 2007); HM is the harmonic mean estimator (Kass and Raftery, 1995). “IS x ” corresponds to an importance sampling estimate where the proposal density is a convex combination of the prior and posterior, with $100(x/10)\%$ of the proposal samples coming from the prior and $100(1-x/10)\%$ from the posterior (again see Kass and Raftery, 1995).

on the variogram analysis in Section 2, we choose to use a smoothness (ν) which is both constant across segments and fixed to be $\nu = 0.5$, corresponding to an exponential correlation structure in (3.3). Both the hyperparameters and fixed ν apply to all spatial models outlined in Section 6.1.

5.3. *Marginal likelihood estimates, prediction, and computation.* The various methods for estimating the marginal likelihoods (4.5) outlined in Appendix B were applied to the twenty segmentations; the resulting posterior probabilities (4.4) are plotted in Figure 5. While the different methods are not completely consistent (see Newton and Raftery, 1994; Carlin and Chib, 1995; and Raftery et al., 2007), they collectively give

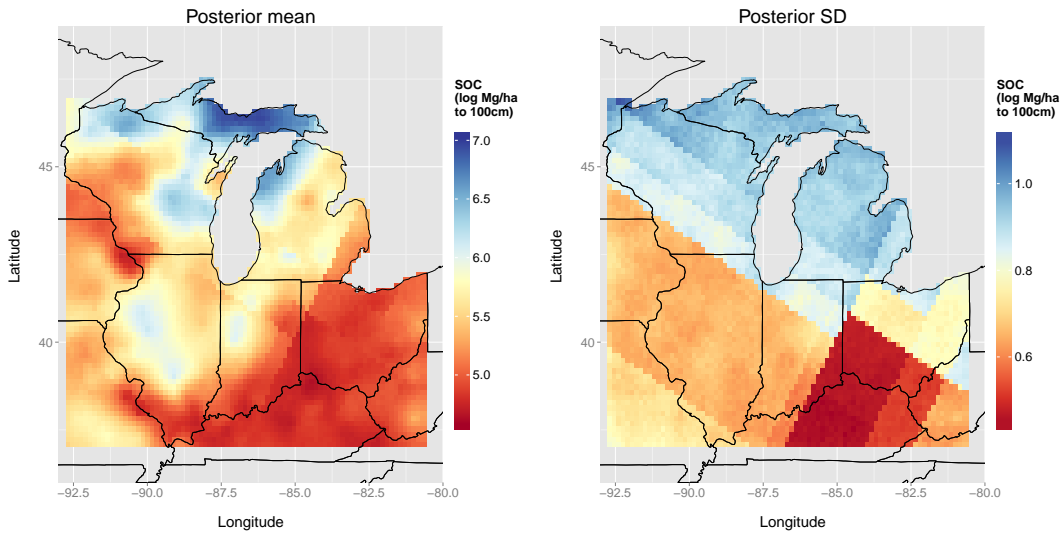


FIG 6. Model-averaged posterior mean predictions (left) and corresponding posterior standard deviations (right) for log SOC in the Great Lakes region, using the HM posterior model probabilities from Figure 5.

non-zero weight to the same three or four segmentations (6, 10, 15, and 16) and none of the methods suggest that the models should be evenly distributed across the twenty segmentations. Based on these similarities, we decided to use the harmonic mean estimator (HM in Figure 5) in spite of its somewhat suboptimal theoretical properties (see, e.g., Chapter 10 of Gilks, Richardson and Spiegelhalter, 1996).

The resulting model-averaged posterior mean prediction map for the Great Lakes region and corresponding posterior standard deviations using the HM posterior model probabilities are shown in Figure 6. In spite of the fact that, under the model averaging, the resulting predicted surface is theoretically smooth, note that the posterior mean predictions are in fact somewhat “blocky,” and the standard deviations even more so. This potentially undesirable lack of smoothness is due to the fact that only three segmentations receive any meaningfully non-zero weight (for the HM estimator: segmentations 6, 10, and 15), and furthermore these segmentations have strong similarities (Figure 4). While this particular prediction map reflects poorly on the ability of the model to produce smooth prediction surfaces, we note that this non-smoothness is what the SOC data select as the best model fits, and again reiterate that the other marginal likelihood estimation methods give qualitatively similar results.

As an illustration of the types of prediction surfaces the model *could have* produced under more uniform posterior model probabilities, consider the prediction map and standard errors shown in Figure 7. The predictions in this plot were drawn us-

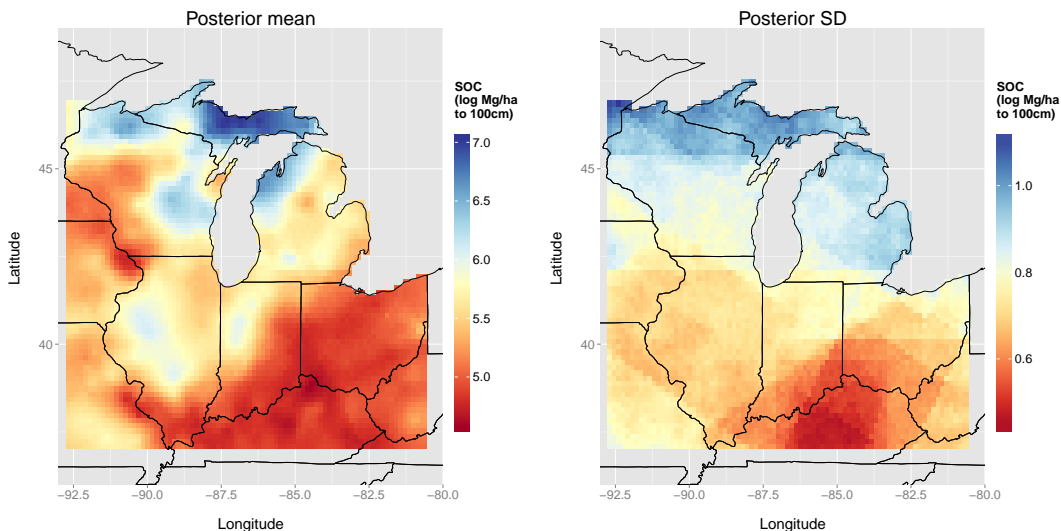


FIG 7. *Model-averaged posterior mean predictions (left) and corresponding posterior standard deviations (right) for log SOC in the Great Lakes region, when each posterior model probability is equal to $1/20 = 0.05$.*

ing uniform model probabilities, in which we fixed each $p(\mathcal{T}_j|\mathbf{Z} = \mathbf{z}) = 1/J = 0.05$. The posterior mean prediction no longer shows any residual features of the underlying independent-across-segments fitted models, and is very similar to the true predictions given in Figure 6. Some residual features of the segmentations are visible in the standard deviation map, but the map is, for all intents and purposes, smooth. Again, we show this map purely for illustrative purposes to highlight the fact that this model can indeed yield smooth prediction surfaces.

Finally, a major benefit of using our nonstationary method with treed covariate segmentations is the significant reduction in computational time relative to fitting a stationary Bayesian spatial model. For a dataset of size $n \approx 800$ observations, the nonstationary model fitting took approximately 10 hours (including the segmentation MCMC and using 20,000 iterations for each of the $J = 20$ segmentation models) while a corresponding stationary model (e.g., S-GP-1; see Section 6.1) took over 60 hours (computational times given are for a 2x Eight Core Xeon 2.66GHz machine with 384GB RAM). These improvements in computational times are due to two factors: first, the likelihood conditional on a segmentation (see (3.5)) is the product of independent multivariate Gaussian likelihoods; second, each of the segmentation models can be fit ahead of time, in parallel.

6. Model comparison.

TABLE 2

A summary of the models fit to the soil carbon data set. (GP indicates a Gaussian process; lat/lon refers to latitude/longitude.) Computational times are approximate and correspond to fitting the model to the full data set of 790 observations.

Label	Details	Mean function	Comp. time
NS-GP	Bayesian nonstationary GP	Constant	10 hours [†]
S-GP-1	Bayesian stationary GP	Constant	61 hours [†]
S-GP-2	Bayesian stationary GP	Lat, lon, lat/lon interaction	61 hours [†]
TGP	(Bayesian) treed GP	Lat/lon for inputs and mean	3.5 hours [†]
BART	Bayesian additive regression trees	Lat/lon as inputs	6 minutes [†]

[†]Time given for a 2x Eight Core Xeon 2.66GHz machine with 384GB RAM, where the MCMC for each model is run for 20000 total iterations.

6.1. *Alternative models.* The model-averaged, segmentation-based nonstationary model (“NS-GP”) is compared with several traditional methods, a summary of which is given in Table 2.

Bayesian stationary Gaussian process. A traditional stationary (anisotropic) spatial Gaussian process model can actually be defined as a special case of the nonstationary model: simply set $K = 1$ (i.e., define a single segment which is equivalent to the spatial domain \mathcal{D}) which implies $J = 1$ (i.e., a single “segmentation”). Two specific stationary models will be used which differ in their mean structure: the first model will have a constant mean over space, i.e., $E[Z(\mathbf{s})] \equiv \mu$ for all $\mathbf{s} \in \mathcal{D}$ (label this model S-GP-1); the second model will have a linear mean function which includes longitude, latitude, and the interaction between latitude and longitude (labelled S-GP-2). The MCMC for both stationary models was run for 20,000 iterations, with 10,000 discarded as burn-in.

Bayesian additive regression trees. Bayesian additive regression trees (BART; Chipman, George and McCulloch, 2010) is a Bayesian sum-of-trees model developed to enhance the more algorithmic ensemble methods. BART has been shown to perform well in a variety of settings, particularly for prediction (see, for example, Bonato et al., 2011; Ding et al., 2012; Green and Kern, 2012). Because of this, we compare predictions from our model to those obtained from BART. In this model, we use latitude and longitude as covariates. We use two R packages: `bartMachine` (Kapelner and Bleich, 2014) and `BayesTree` (Chipman and McCulloch, 2014). For each holdout set, we first used the default settings of the function `bartMachineCV` which makes use of cross validation to identify hyperparameter values (default settings use five-fold cross-validation and searches over a total of 18 combinations of hyperparameter values). We then used the function `bart` from `BayesTree` to fit BART using the previously identified optimal hyperparameter values for a total of 20,000 iterations, using 10,000 as burn-in. Although we could have also fit BART using the function `bartMachine`

and thus use only one R package, the function `bart` returns posterior draws from the posterior distributions of the predicted values for both the training and test data sets which we used to compute the CRPS (see Section 6.2).

Treed Gaussian process. Based on the similarities of our approach and the treed Gaussian process (TGP) model of Gramacy and Lee (2008), we also compare our method to TGP. Implementing this model is extremely straightforward using the `btgp` function in the `tgp` package for R (Gramacy, 2007). A total of 20,000 MCMC iterations were used, with 10,000 burn-in iterations and no thinning of the chain. Similar to the other spatial models, the underlying correlation model was set to be exponential; all other defaults were used, including a mean function with the main effects of latitude and longitude.

6.2. *Evaluation criteria.* Before proceeding with the model comparison, we briefly introduce several out-of-sample and in-sample criteria to be used for model evaluation.

Out-of-sample criteria. Cross-validation criteria are emphasized because, again, our primary goal is to improve the quality of SOC spatial predictions. As such, 10 percent of the observations in our data set will be held out and used as test data (with m total observations), while the remaining 90 percent of the observations will be used as training data to fit each model and predict at the m test data locations.

The out-of-sample evaluation criteria used to compare predictions with the held-out data for each of the models are the mean squared prediction error (MSPE), the continuous rank probability score (CRPS; Gneiting and Raftery, 2007), and the log score (logS; Good, 1952). The MSPE is simply $MSPE = m^{-1} \sum_{j=1}^m (z_j^* - \hat{z}_j^*)^2$, where z_j^* is the j th held-out observed value and \hat{z}_j^* is the corresponding predicted posterior mean. Krüger et al. (2016) outline several methods for estimating the CRPS and logS for individual predictions based on the output from MCMC algorithms (i.e., \widehat{CRPS}_j and $\widehat{\log S}_j$ for $j = 1, \dots, m$); then, the mean scores

$$\widehat{CRPS} = m^{-1} \sum_{j=1}^m \widehat{CRPS}_j, \quad \widehat{\log S} = m^{-1} \sum_{j=1}^m \widehat{\log S}_j$$

are calculated for the test set and compared across models. Unfortunately, the conditional predictive cumulative distribution functions (conditional on the true parameter state, i.e., the likelihood) are not available for BART and TGP, so we instead use what Krüger et al. (2016) call the empirical CDF method (ECDF) for calculating CRPS for each model. ECDF is based on samples drawn from the posterior predictive distribution (e.g., (4.1) and the PPA) and is a consistent approximation for the CRPS for every predictive distribution with finite mean (Krüger et al., 2016). For logS, the lack of a likelihood for TGP and BART means that we instead must resort to a kernel

density estimate of the predictive density, again based on samples from the posterior predictive distribution, which is consistent for logS under slightly more restrictive conditions (Krüger et al., 2016). In order to ensure comparability across the models, we use the kernel density estimate for S-GP-1, S-GP-2, and NS-GP (even though the conditional CDF is available for these models; see (4.2)). The ECDF estimate of CRPS is calculated using the `scoringRules` package (Jordan, Krüger and Lerch, 2016), while the kernel density estimate of logS is calculated using the equations outlined in Section 3.3 of Krüger et al. (2016).

Since the evaluation of each of the out-of-sample criteria is likely to be at least somewhat sensitive to the choice of a particular holdout sample, in practice we actually fit each model multiple times using a different holdout sample for each fit. As a summary, we present box plots to display the distribution of each evaluation criteria across holdout samples.

In-sample criteria. In addition to the out-of-sample criteria, we also assess the in-sample fit of each model in order to determine the appropriateness of the statistical model. For this comparison, we fit each model in Table 2 to the full data set and computed predictions within-sample. We used in-sample versions of MSE, CRPS, and log score, calculated as with the out-of-sample criteria.

6.3. *Results.* Each of the models in Table 2 were fit to the full data set as well as 20 different holdout sets. Each holdout set was generated by randomly selecting 10 percent of the locations to be withheld. The out-of-sample criteria are aggregated over the holdout sets and summarized with box plots in Figure 8; also, a summary of the best model for each holdout set across the scoring rules is shown. The average out-of-sample criteria are given in Table 3, and the in-sample criteria (calculated using the full data set with no holdout locations) are summarized in Table 4.

Our nonstationary treed covariate segmentation model is the clear winner for the in-sample criteria, providing major improvements for each criteria. The picture is somewhat less clear for the out-of-sample criteria: while CRPS for NS-GP is better, on average, than the other models, the MSPE for NS-GP is nearly equal to that of the other spatial models. Furthermore, the logS is actually worse (on average) for NS-GP than even BART, although this may be due to several large logS values for NS-GP (note that the distribution of logS over holdout sets for TGP is also skewed). In terms of a holdout set by holdout set comparison, the NS-GP model is most often selected as the best for CRPS and logS (12 and 11 out of 20, respectively) while tying S-GP-1 in terms of MSPE with 7 out of 20 (see the rightmost panel of Figure 8). In general, however, the improvements in Table 3 are small and the box plots for NS-GP in Figure 8 are not significantly different than the other models (other than, perhaps, BART).

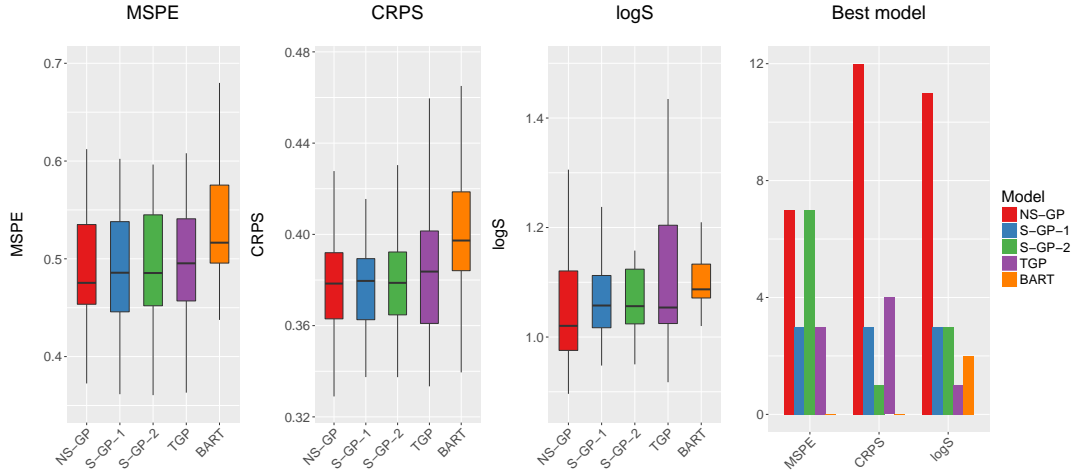


FIG 8. Out-of-sample MSPE, CRPS, and $\log S$ summarized across the twenty holdout sets, as well as a tabulation of the best model for each holdout set across scoring rules. Note: each scoring rule is negatively oriented, i.e., a lower score indicates a better prediction.

TABLE 3

Mean out-of-sample criteria (averaged over the holdout sets), with the best score for each criteria in bold. Note: lower scores indicate better performance.

Model	MSPE	% change	CRPS	% change	logS	% change
NS-GP	0.5094	–	0.3826	–	1.181	–
S-GP-1	0.5069	–0.5%	0.3861	+1.0%	1.092	–7.5%
S-GP-2	0.5084	–0.2%	0.3868	+1.1%	1.093	–7.4%
TGP	0.5174	+1.6%	0.3905	+2.1%	1.182	+0.1%
BART	0.5466	+7.3%	0.4047	+5.8%	1.118	–5.4%

TABLE 4

In-sample evaluation criteria (for the full data set), with the best score for each criteria in bold. Note: lower scores indicate better performance.

Model	MSE	% change	CRPS	% change	logS	% change
NS-GP	0.3482	–	0.3214	–	0.8758	–
S-GP-1	0.3738	+7.3%	0.3372	+5.0%	0.9590	+9.5%
S-GP-2	0.3785	+8.7%	0.3393	+5.6%	0.9570	+9.3%
TGP	0.4080	+17.2%	0.3467	+7.9%	0.9699	+10.7%
BART	0.4521	+29.8%	0.3702	+15.2%	1.0313	+17.8%

7. Discussion. In this paper, we have proposed a novel method for obtaining predictions of soil organic carbon at unobserved locations using a covariate-driven nonstationary spatial Gaussian process model. Our approach uses an underlying treed

or segmentation process to partition geographic space according to the within-partition distribution of the covariates (here, land use-land cover and drainage class), so that the covariates indirectly inform the modeled first- and second-order properties of SOC as well as the resulting predictions. This approach extends existing covariate-driven nonstationary approaches in that the information a covariate provides on SOC can be used for prediction even if the covariate is not fully observed over the spatial domain. Bayesian model averaging accounts for uncertainty in the segmentation process as well as allows for more than one covariate to inform the first- and second-order properties of SOC. Our approach yields strong gains for in-sample evaluation criteria and modest gains for out-of-sample criteria. Furthermore, while many nonstationary spatial approaches are computationally intensive, our approach results in computational times that are significantly faster than the time required to fit a corresponding second-order stationary model.

Of course, there are several limitations to our nonstationary model for SOC. First, the marginal likelihood estimation seems to be fairly sensitive to individual likelihood values, resulting in a few non-zero and many (nearly) zero posterior model probabilities. As such, while the model-averaged prediction surface is theoretically smooth, in practice the mean surface is rather un-smooth (as are the standard errors). Also, while our nonstationary model clearly improves in-sample metrics, the improvements in out-of-sample prediction are modest. This observation is perhaps reflective of the SOC sampling design, in that spatially-redundant information is not collected.

Finally, while Bayesian CART provides a convenient method for partitioning the geographic space, the fact that it can only generate segmentations with square corners is somewhat limiting. In theory there should be no reason to require that the spatial regions for which the covariates are homogeneous to be rectangular, especially for an environmental process like SOC. For this reason, other clustering or segmentation methods could be considered; however, our model averaging approach requires an informative prior over the space of all possible segmentations, which can be straightforwardly obtained from the Bayesian CART posterior but might not be so easily obtained from other approaches.

APPENDIX A: TREED COVARIATE MODELS VIA BAYESIAN CART

The following Bayesian classification and regression trees (Bayesian CART, [Chipman, George and McCulloch, 1998](#)) algorithm is used to obtain posterior samples of a treed process based on covariate variables, which we will use to specify the prior distribution $p(\mathcal{T})$ introduced in Section 3. Formally, define $z_T(\mathbf{s})$ to be a scalar covariate observed at a set of locations $\{\mathbf{s}'_1, \dots, \mathbf{s}'_m\}$, which may or may not coincide with the monitoring sites for the spatial process $\{\mathbf{s}_1, \mathbf{s}_2, \dots, \mathbf{s}_n\}$ and may also not be available at all prediction locations of interest (and, therefore, the raw values can not be used directly in the mean structure for the model outlined in Section 3). Collect the

observed covariate values into the vector $\mathbf{Z}_T = (z_T(\mathbf{s}'_1), \dots, z_T(\mathbf{s}'_m))^\top$. While \mathbf{Z} is used previously to denote the observed values of the spatial process of interest, here we use \mathbf{Z}_T to denote the “treed response,” or the variable that will be used as the response for the treed model. Following the notation of [Chipman, George and McCulloch \(1998\)](#), a Bayesian CART model defines a conditional distribution of the treed response \mathbf{Z}_T given the set of predictors (here, $\{\mathbf{s}'_1, \dots, \mathbf{s}'_m\}$) and involves two primary components: first, the tree \mathcal{T} with K terminal nodes (also called segments or subregions), and second, a parameter $\boldsymbol{\theta}_T = (\boldsymbol{\theta}_T^{(1)}, \dots, \boldsymbol{\theta}_T^{(K)})$ that associates the parameter $\boldsymbol{\theta}_T^{(k)}$ with the k th terminal node (also note the distinction between $\boldsymbol{\theta}_k$ from [Section 3](#) and $\boldsymbol{\theta}_T^{(k)}$). The treed response values are similarly associated with the terminal nodes by re-indexing the individual values so that $z_T^{(k,j)}$ corresponds to the j th observation of $z_T(\cdot)$ in the k th partition. In the simplest form of CART, it is usually assumed that, conditional on $(\boldsymbol{\theta}_T, \mathcal{T})$, values of the treed response within a terminal node are independent and identically distributed (iid), and values of the treed response are independent across partitions. Therefore, the CART model distribution for the treed response can be written as

$$p(\mathbf{Z}_T | \boldsymbol{\theta}_T, \mathcal{T}) = \prod_{k=1}^K \prod_{j=1}^{n_k} p(z_T^{(k,j)} | \boldsymbol{\theta}_T^{(k)}).$$

After the CART model has been specified conditional on $(\boldsymbol{\theta}_T, \mathcal{T})$, a Bayesian analysis continues with a specification of the prior distribution $p(\boldsymbol{\theta}_T, \mathcal{T})$. And, because $\boldsymbol{\theta}_T$ indexes a parametric model for each \mathcal{T} , it is helpful to use the conditional prior $p(\boldsymbol{\theta}_T, \mathcal{T}) = p(\boldsymbol{\theta}_T | \mathcal{T})p(\mathcal{T})$. The specification of the tree prior $p(\mathcal{T})$ is outlined in [Chipman, George and McCulloch \(1998\)](#) implicitly as a tree-generating stochastic process. Drawing from the prior intuitively involves starting with a tree consisting of a single node, and then growing sequentially by recursively enforcing binary splits on the terminal nodes. Starting with \mathcal{T} as the trivial tree consisting of a single root (and terminal) node, denoted η_0 , the algorithm proceeds as follows:

1. **Split** the terminal node η_0 into η_1 and η_2 with probability $p_S(\eta_0, \mathcal{T})$.
2. If the node splits, assign a splitting **rule** ρ_0 according to a distribution $p_R(\rho_0 | \eta_0, \mathcal{T})$.

Let \mathcal{T} be the new tree; repeat steps 1 and 2 as needed or as possible to each terminal node of \mathcal{T} . [Chipman, George and McCulloch \(1998\)](#) recommend $p_S(\eta_i, \mathcal{T}) = \alpha_T(1 + d_i)^{-\beta_T}$, where $0 \leq \alpha_T \leq 1$, $\beta_T \geq 0$, and d_i is the depth of node η_i (i.e., the number of splits above η_i), and setting $p_R(\rho_i | \eta_i, \mathcal{T})$ be the uniform distribution over the finite (observed) predictor space. Finally, [Chipman, George and McCulloch \(1998\)](#) recommend choosing priors for which it is possible to integrate out the tree parameter $\boldsymbol{\theta}_T$ and obtain a closed form for the distribution of the response given the tree.

When the tree parameter $\boldsymbol{\theta}_T$ can be marginalized to give a closed form for the

marginal likelihood $p(\mathbf{Z}_T|\mathcal{T})$, the only remaining unknown is the tree process \mathcal{T} , which has the posterior $p(\mathcal{T}|\mathbf{Z}_T) \propto p(\mathbf{Z}_T|\mathcal{T}) \cdot p(\mathcal{T})$. While the tree prior distribution is discrete, the number of possible trees makes analytic calculation of the posterior unfeasible (except in trivial cases). Therefore, we instead resort to Markov chain Monte Carlo (MCMC) methods using a Metropolis-Hastings algorithm to simulate a sequence of trees $\mathcal{T}_0, \mathcal{T}_1, \mathcal{T}_2, \dots$ that converges in distribution to the posterior $p(\mathcal{T}|\mathbf{Z}_T)$. The details of this algorithm have been well-developed in the literature (see, e.g., [Chipman, George and McCulloch, 1998](#) or [Gramacy and Lee, 2008](#); also, [Kapelner and Bleich, 2014](#) provides a very helpful summary). In general, moving from the current tree, say \mathcal{T}^i , to a proposed tree, \mathcal{T}^* , is accepted with probability

$$\alpha(\mathcal{T}^i, \mathcal{T}^*) = \min \left\{ \frac{p(\mathbf{Z}_T|\mathcal{T}^*) \cdot p(\mathcal{T}^*) \cdot q(\mathcal{T}^*, \mathcal{T}^i)}{p(\mathbf{Z}_T|\mathcal{T}^i) \cdot p(\mathcal{T}^i) \cdot q(\mathcal{T}^i, \mathcal{T}^*)}, 1 \right\},$$

where $q(\mathcal{T}^*, \mathcal{T}^i)$ represents the transition kernel or probability of moving from the current tree \mathcal{T}^i to the proposed tree \mathcal{T}^* ; otherwise, the proposed tree is rejected. [Chipman, George and McCulloch \(1998\)](#) originally outlined four transition kernels (“grow,” “prune,” “change,” and “swap”); following [Kapelner and Bleich \(2014\)](#), we simply used the kernels “grow,” “prune,” and a modified version of the “change” kernel.

APPENDIX B: MARGINAL LIKELIHOOD ESTIMATION

B.1. Importance sampling techniques. The original citations for what follows are [Rosenkranz \(1992\)](#), [Newton and Raftery \(1994\)](#), [Carlin and Chib \(1995\)](#); however, a helpful summary is provided by Raftery in Chapter 10 (section 3) of [Gilks, Richardson and Spiegelhalter \(1996\)](#).

Recall from (4.5) that the marginal likelihood of interest is

$$p(\mathbf{Z}|\mathcal{T}_j) = \int p(\mathbf{Z}|\boldsymbol{\mu}, \boldsymbol{\theta}, \mathcal{T}_j) p(\boldsymbol{\mu}, \boldsymbol{\theta}|\mathcal{T}_j) d\boldsymbol{\theta} d\boldsymbol{\mu}.$$

What follows is an approach to estimate the marginal likelihood for a single tree, so for simplicity we suppress the implicit dependence on \mathcal{T}_j ; also, in an abuse of notation, rewrite $\boldsymbol{\theta} = (\boldsymbol{\mu}, \boldsymbol{\theta})$. What we want is $p(\mathbf{Z}) = \int L(\boldsymbol{\theta}) \pi(\boldsymbol{\theta}) d\boldsymbol{\theta}$, where $\pi(\boldsymbol{\theta})$ is the prior distribution and $L(\boldsymbol{\theta}) \equiv p(\mathbf{Z}|\boldsymbol{\theta})$ is the likelihood. Furthermore, define

$$\|X\|_h = \frac{1}{T} \sum_{t=1}^T X(\boldsymbol{\theta}^{(t)}),$$

where $\{\boldsymbol{\theta}^{(t)} : t = 1, \dots, T\}$ are samples from the density $h(\boldsymbol{\theta}) / \int h(\boldsymbol{\phi}) d\boldsymbol{\phi}$. Importance sampling supposes we can sample $\boldsymbol{\theta}$ from $cg(\boldsymbol{\theta})$, where $c^{-1} = \int g(\boldsymbol{\theta}) d\boldsymbol{\theta}$; then

$$p(\mathbf{Z}) = \int L(\boldsymbol{\theta}) \pi(\boldsymbol{\theta}) d\boldsymbol{\theta} = \int L(\boldsymbol{\theta}) \left[\frac{\pi(\boldsymbol{\theta})}{cg(\boldsymbol{\theta})} \right] cg(\boldsymbol{\theta}) d\boldsymbol{\theta}.$$

Given $\{\boldsymbol{\theta}^{(t)} : t = 1, \dots, T\}$ from $c \cdot g(\boldsymbol{\theta})$, then

$$(B.1) \quad \hat{p}(\mathbf{Z}) = \frac{1}{T} \sum_{t=1}^T \frac{L(\boldsymbol{\theta}^{(t)})\pi(\boldsymbol{\theta}^{(t)})}{cg(\boldsymbol{\theta}^{(t)})} \equiv \left\| \frac{L\pi}{cg} \right\|_g.$$

If c is unknown, it can be estimated similarly by $\hat{c} = \|\pi/g\|_g$, so that (B.1) becomes $\hat{p}(\mathbf{Z}) = \|L\pi/g\|_g / \|\pi/g\|_g$.

As a simple option, [Newton and Raftery \(1994\)](#) suggest using $g = L\pi$ (i.e., the posterior $p(\boldsymbol{\theta}|\mathbf{Z})$) since posterior simulation already provides samples from this choice of g . In this case,

$$(B.2) \quad \hat{p}_{HM}(\mathbf{Z}) = \frac{1}{\|1/L\|_{\text{post}}}$$

where “post” indicates that the samples of $\boldsymbol{\theta}$ are from the posterior (the “HM” subscript indicates that this is the harmonic mean of the likelihood values). This estimator converges almost surely to $p(\mathbf{Z})$ as $T \rightarrow \infty$, but does not satisfy a Gaussian CLT since the variance of $1/\hat{p}_{HM}(\mathbf{Z})$ is usually non-finite. However, [Rosenkranz \(1992\)](#) concludes that this estimator is a good choice because it is easy to compute and performs well when T is large ($\geq 5,000$), a result reiterated by [Carlin and Chib \(1995\)](#).

More generally, g can be $g_\delta(\boldsymbol{\theta}) = \delta \cdot \pi(\boldsymbol{\theta}) + [1 - \delta] \cdot p(\boldsymbol{\theta}|\mathbf{Z})$ ([Newton and Raftery, 1994](#)), where $0 < \delta < 1$ and $p(\boldsymbol{\theta}|\mathbf{Z})$ is the posterior distribution, because the mixture of the prior and posterior yields high efficiency and satisfies a Gaussian CLT. To avoid having to simulate from the prior as well as the posterior, one can simulate T values of $\boldsymbol{\theta}$ from the posterior and suppose that an additional $\delta T/(1 - \delta)$ values are drawn from the prior, each of which has a likelihood $L(\boldsymbol{\theta})$ equal to its expected value $p(\mathbf{Z})$. Then, the estimate $\hat{p}_\delta(\mathbf{Z})$ can be obtained by finding the solution x to the equation

$$x = \frac{\frac{\delta T}{1-\delta} + \sum_{t=1}^T \frac{L(\boldsymbol{\theta}^{(t)})}{\delta x + (1-\delta)L(\boldsymbol{\theta}^{(t)})}}{\frac{\delta T}{x(1-\delta)} + \sum_{t=1}^T [\delta x + (1-\delta)L(\boldsymbol{\theta}^{(t)})]^{-1}}$$

where the $\{\boldsymbol{\theta}^{(t)} : t = 1, \dots, T\}$ are the posterior samples (page 169, Chapter 10, [Gilks, Richardson and Spiegelhalter, 1996](#)), which can be done using an iterative Newton-Raphson scheme. [Rosenkranz \(1992\)](#) found that large values of δ (i.e., near 1) yield the best performance.

B.2. Monte Carlo approximations to AIC and BIC. [Raftery et al. \(2007\)](#) present a variety of methods for estimating the marginal likelihood using only the likelihoods from posterior simulation output. In fact, their work specifically aims to improve the instability (i.e., infinite asymptotic variance) of the harmonic mean estimator (B.2).

One of the approaches in [Raftery et al. \(2007\)](#) is based on the fact that the posterior distribution of the log likelihood approximately follows a gamma distribution. As such, they note that the corresponding estimate of the marginal likelihood has an interesting similarity to the Bayesian information criterion (BIC), which yields a Monte Carlo approximation to the log marginal likelihood (henceforth BICM)

$$\log \hat{p}_{\text{BICM}}(\mathbf{Z}) = \bar{\mathcal{L}} - s_{\mathcal{L}}^2(\log n - 1),$$

where $\bar{\mathcal{L}}$ and $s_{\mathcal{L}}^2$ are the sample mean and variance of the log likelihoods from the posterior samples and n is the sample size. Similarly, a posterior simulation-based version of Akaike's information criterion (AIC) can be used to approximate the log marginal likelihood (henceforth AICM)

$$\log \hat{p}_{\text{AICM}}(\mathbf{Z}) = 2(\bar{\mathcal{L}} - s_{\mathcal{L}}^2).$$

ACKNOWLEDGEMENTS

This work was supported in part by the Statistical Methods for Atmospheric and Oceanic Sciences (STATMOS) research network (NSF-DMS awards 1106862, 1106974, and 1107046). C. A. Calder was also partially supported by NSF-DMS award 1209161.

REFERENCES

- ADLER, R. J. (1981). *The Geometry of Random Fields*. John Wiley & Sons.
- BATJES, N. H. (1996). Total carbon and nitrogen in the soils of the world. *European Journal of Soil Science* **47** 151–163.
- BEAUDETTE, D. E. and SKOVLIN, J. M. (2015). `soilDB`: Soil Database Interface R package version 1.5-2.
- BLISS, N. B., WALTMAN, S. W., WEST, L. T., NEALE, A. and MEHAFFEY, M. (2014). Distribution of Soil Organic Carbon in the Conterminous United States. In *Soil Carbon*, (A. E. Hartemink and K. McSweeney, eds.). *Progress in Soil Science* 85-93. Springer International Publishing.
- BOCHNER, S. (1959). *Lectures on Fourier integrals. No. 42*. Princeton University Press.
- BONATO, V., BALADANDAYUTHAPANI, V., BROOM, B. M., SULMAN, E. P., ALDAPE, K. D. and DO, K.-A. (2011). Bayesian ensemble methods for survival prediction in gene expression data. *Bioinformatics* **27** 359–367.
- CALDER, C. A. (2008). A dynamic process convolution approach to modeling ambient particulate matter concentrations. *Environmetrics* **19** 39–48.
- CARLIN, B. P. and CHIB, S. (1995). Bayesian Model Choice via Markov Chain Monte Carlo Methods. *Journal of the Royal Statistical Society. Series B (Methodological)* **57** pp. 473-484.
- CHIPMAN, H. A., GEORGE, E. I. and MCCULLOCH, R. E. (1998). Bayesian CART Model Search. *Journal of the American Statistical Association* **93** 935-948.
- CHIPMAN, H. A., GEORGE, E. I. and MCCULLOCH, R. E. (2010). BART: Bayesian Additive Regression Trees. *The Annals of Applied Statistics* **4** 266-298.
- CHIPMAN, H. and MCCULLOCH, R. (2014). `BayesTree`: Bayesian Additive Regression Trees R package version 0.3-1.2.
- DING, J., BASHASHATI, A., ROTH, A., OLOUMI, A., TSE, K., ZENG, T., HAFFARI, G., HIRST, M., MARRA, M. A., CONDON, A., APARICIO, S. and SHAH, S. P. (2012). Feature-based classifiers for somatic mutation detection in tumour-normal paired sequencing data. *Bioinformatics* **28** 167–175.

- FUENTES, M. (2001). A high frequency kriging approach for non-stationary environmental processes. *Environmetrics* **12** 469–483.
- GELMAN, A. (2006). Prior distributions for variance parameters in hierarchical models (comment on article by Browne and Draper). *Bayesian Analysis* **1** 515–534.
- GILKS, W. R., RICHARDSON, S. and SPIEGELHALTER, D. J. (1996). *Markov Chain Monte Carlo in Practice*. Chapman & Hall.
- GNEITING, T. and RAFTERY, A. E. (2007). Strictly Proper Scoring Rules, Prediction, and Estimation. *Journal of the American Statistical Association* **102** 359–378.
- GOIDTS, E. and VAN WESEMAEL, B. (2007). Regional assessment of soil organic carbon changes under agriculture in Southern Belgium, 1955–2005. *Geoderma* **141** 341 - 354.
- GOOD, I. J. (1952). Rational Decisions. *Journal of the Royal Statistical Society. Series B (Methodological)* **14** pp. 107–114.
- GRAMACY, R. B. (2007). tgp: An R Package for Bayesian Nonstationary, Semiparametric Nonlinear Regression and Design by Treed Gaussian Process Models. *Journal of Statistical Software* **19** 1–46.
- GRAMACY, R. B. and LEE, H. K. H. (2008). Bayesian Treed Gaussian Process Models With an Application to Computer Modeling. *Journal of the American Statistical Association* **103** 1119–1130.
- GREEN, D. P. and KERN, H. L. (2012). Modeling Heterogeneous Treatment Effects in Survey Experiments with Bayesian Additive Regression Trees. *Public Opinion Quarterly* **76** 491–511.
- HIGDON, D. (1998). A process-convolution approach to modelling temperatures in the North Atlantic Ocean. *Environmental and Ecological Statistics* **5** 173–190.
- INGEBRIGTSEN, R., LINDGREN, F. and STEINSLAND, I. (2014). Spatial models with explanatory variables in the dependence structure. *Spatial Statistics* **8** 20 - 38.
- JOBBÁGY, E. G. and JACKSON, R. B. (2000). The Vertical Distribution of Soil Organic Carbon and its Relationship to Climate and Vegetation. *Ecological Applications* **10**.
- JORDAN, A., KRÜGER, F. and LERCH, S. (2016). scoringRules: Scoring Rules for Parametric and Simulated Distribution Forecasts R package version 0.9.
- KAPELNER, A. and BLEICH, J. (2014). bartMachine: Machine Learning With Bayesian Additive Regression Trees. *ArXiv e-prints*.
- KASS, R. E. and RAFTERY, A. E. (1995). Bayes Factors. *Journal of the American Statistical Association* **90** 773–795.
- KATZFUSS, M. (2013). Bayesian nonstationary spatial modeling for very large datasets. *Environmetrics* **24** 189–200.
- KRÜGER, F., LERCH, S., THORARINSDOTTIR, T. and GNEITING, T. (2016). Probabilistic Forecasting and Comparative Model Assessment Based on Markov Chain Monte Carlo Output. *ArXiv pre-prints*.
- LINDGREN, F., RUE, H. and LINDSTROM, J. (2011). An explicit link between Gaussian fields and Gaussian Markov random fields: the stochastic partial differential equation approach. *Journal of the Royal Statistical Society: Series B (Statistical Methodology)* **73** 423–498.
- MEERSMANS, J., RIDDER, F. D., CANTERS, F., BAETS, S. D. and MOLLE, M. V. (2008). A multiple regression approach to assess the spatial distribution of Soil Organic Carbon (SOC) at the regional scale (Flanders, Belgium). *Geoderma* **143** 1 - 13.
- MINASNY, B., MCBRATNEY, A. B., MENDONÇA-SANTOS, M. L., ODEH, I. O. A. and GUYON, B. (2006). Prediction and digital mapping of soil carbon storage in the Lower Namoi Valley. *Soil Research* **44** 233–244.
- MISHRA, U., LAL, R., SLATER, B., CALHOUN, F., LIU, D. and VAN MEIRVENNE, M. (2009). Predicting Soil Organic Carbon Stock Using Profile Depth Distribution Functions and Ordinary Kriging. *Soil Science Society of America Journal* **73** 614–621.
- NEWTON, M. A. and RAFTERY, A. E. (1994). Approximate Bayesian Inference with the Weighted Likelihood Bootstrap. *Journal of the Royal Statistical Society. Series B (Methodological)* **56** pp.

- 3-48.
- PACIOREK, C. J. and SCHERVISH, M. J. (2006). Spatial modeling using a new class of nonstationary covariance functions. *Environmetrics* **17** 483-506.
- POST, W. M. and KWON, K. C. (2000). Soil carbon sequestration and land-use change: processes and potential. *Global Change Biology* **6** 317-327.
- POST, W. M., EMANUEL, W. R., ZINKE, P. J. and STANGENBERGER, A. (1982). Soil carbon pools and world life zones. *Nature* **298** 156-159.
- RAFTERY, A. E., NEWTON, M. A., SATAGOPAN, J. M. and KRIVITSKY, P. N. (2007). Estimating the integrated likelihood via posterior simulation using the harmonic mean identity. *Bayesian Statistics* **8** 1-45.
- REICH, B. J., EIDSVIK, J., GUINDANI, M., NAIL, A. J. and SCHMIDT, A. M. (2011). A class of covariate-dependent spatiotemporal covariance functions for the analysis of daily ozone concentration. *The Annals of Applied Statistics* **5** 2425-2447.
- RISSER, M. D. and CALDER, C. A. (2015). Regression-based covariance functions for nonstationary spatial modeling. *Environmetrics* **26** 284-297.
- ROSENKRANZ, S. (1992). The Bayes factor for model evaluation in a hierarchical Poisson model for area counts PhD thesis, University of Washington.
- SAMPSON, P. D. and GUTTORP, P. (1992). Nonparametric Estimation of Nonstationary Spatial Covariance Structure. *Journal of the American Statistical Association* **87** 108-119.
- SCHMIDT, A. M., GUTTORP, P. and O'HAGAN, A. (2011). Considering covariates in the covariance structure of spatial processes. *Environmetrics* **22** 487-500.
- SIMBAHAN, G. C., DOBERMANN, A., GOOVAERTS, P., PING, J. and HADDIX, M. L. (2006). Fine-resolution mapping of soil organic carbon based on multivariate secondary data. *Geoderma* **132** 471 - 489.
- SLEUTEL, S., DE NEVE, S., HOFMAN, G., BOECKX, P., BEHEYDT, D., VAN CLEEMPUT, O., MESTDAGH, I., LOOTENS, P., CARLIER, L., VAN CAMP, N., VERBEECK, H., VANDE WALLE, I., SAMSON, R., LUST, N. and LEMEUR, R. (2003). Carbon stock changes and carbon sequestration potential of Flemish cropland soils. *Global Change Biology* **9** 1193-1203.
- SOLOMAN, S. (2007). Climate Change 2007: The physical science basis. *International Panel on Climate Change* **4**.
- VIANNA NETO, J. H., SCHMIDT, A. M. and GUTTORP, P. (2014). Accounting for spatially varying directional effects in spatial covariance structures. *Journal of the Royal Statistical Society: Series C (Applied Statistics)* **63** 103-122.
- WILLS, S., SEQUEIRA, C., LOECKE, T., BENHAM, E., FERGUSON, R., SCHEFFE, K. and WEST, L. (2013). Rapid Carbon Assessment (RaCA) Methodology Sampling and Initial Summary United States Department of Agriculture, Natural Resources Conservation Service. Available online at http://www.nrcs.usda.gov/Internet/FSE_DOCUMENTS/nrcs142p2_052841.pdf.

CLIMATE & ECOSYSTEM SCIENCES DIVISION
LAWRENCE BERKELEY NATIONAL LABORATORY
1 CYCLOTRON ROAD
BERKELEY, CA 94720
E-MAIL: mdrisser@lbl.gov

DEPARTMENT OF BIOSTATISTICS
UNIVERSITY OF MICHIGAN
M4525 SPH II
1415 WASHINGTON HEIGHTS
ANN ARBOR, MI 48109
E-MAIL: berrocal@umich.edu

DEPARTMENT OF STATISTICS
THE OHIO STATE UNIVERSITY
429 COCKINS HALL
1958 NEIL AVENUE
COLUMBUS, OH 43210
E-MAIL: calder@stat.osu.edu

DEPARTMENT OF STATISTICS
BRIGHAM YOUNG UNIVERSITY
216 TMCB
PROVO, UT 84602
E-MAIL: cberrett@stat.byu.edu